Korean J. Chem. Eng., 36(5), 800-806 (2019)
DOI: 10.1007/s11814-019-0246-6

pISSN: 0256-1115
eISSN: 1975-7220

Highly stretchable and sensitive strain sensors based on single-walled carbon nanotube-coated nylon textile

Yein Lee*,‡, Juhyeon Kim*,‡, Heeseon Hwang, and Soo-Hwan Jeong*,†**

*Department of Chemical Engineering, Kyungpook National University (KNU), 80 Daehak-ro, Buk-gu, Daegu 41566, Korea
**Korea Institute of Robot and Convergence, 39 Jigok-ro, Nam-gu, Pohang-si, Gyeongsangbuk-do 37666, Korea
(*Received 22 October 2018 • accepted 21 February 2019*)

Abstract−With increasing demand for wearable electronic devices, strain sensor development with a high stretchability becomes quite critical. To develop a high performance stretchable strain sensor, we used nylon textile obtained from commercial thigh-highs as substrate for coating single-walled CNT (SWNT). Using vacuum-assisted spray-layer-by-layer technique, SWNTs were uniformly coated on the surface of textile fibers. Our SWNT/nylon textile sensor exhibited high sensitivity of 72 gauge factor at 100% strain, fast response, and excellent durability. In addition, the sensors were used for human motion detection by attaching to glove and sewing with leggings. We have a great expectation that high stretchability, sensitivity, and durability of this SWNT/nylon textile strain sensor, with its simple integration to clothing, opens up new opportunities for fabrication of high performance wearable strain sensor.

Keywords: Carbon Nanotube, Nylon Textile, Strain Sensor, Spray-layer-by-layer

INTRODUCTION

Tremendous research efforts have been devoted to developing wearable and stretchable strain sensors for the potential applications of human motion detection, personalized heal monitoring, sport monitoring, and rehabilitation treatment [1-4]. Generally, wearable and stretchable strain sensors consist of conducting nanomaterials, such as conducting polymers [5,6], metal nanowires [7,8], graphene [9-11] and carbon nanotubes (CNT) [12-14], imbedded in or attached on the stretchable polymers.

Among conducting nanomaterials, CNT is most promising candidate due to its outstanding mechanical and electrical properties. It also shows an ultrahigh piezoresistivity, which is known as change in the resistance of materials caused by the structural deformations, due to its chirality [15]: piezoresistive gauge factors of up to 2900 for single-walled CNT (SWNT) [16]. Most of the CNT-based stretchable strain sensors have been prepared by coating CNT solution or laying film/fiber onto elastomer substrates, such as polydimethylsiloxane (PDMS), Ecoflex, and polyurethane (PU). These sensors exhibit high stretchability of >80% and moderate sensitivity (gauge factors of 0.06-69) [12,17-23]. However, the elastomer-based sensors have some drawbacks. Due to the viscoelastic property of elastomer, hysteresis behavior and response delay can be observed and they exhibit the long recovery time [24,25]. In addition, when they should be attached to skin or clothes, solid tapes or rubber pastes are used or they are strapped to prevent the sensors from detaching, resulting in limited comfort.

Therefore, textile-based sensors are highly desirable for wearable strain sensors. The textile-based sensors can be easily integrated to clothes, and then, they are close to the body with comfort and worn almost all the time. In general, they can be fabricated by knitting conducting yarns to produce textile structure [26,27], or coating a textile with conductive materials [28-31]. The coating method is often used to integrate CNT with the textile for fabricating CNT-based strain sensors because it is simple and easily scalable [30]. SWNT-coated cotton yarn [28] and textile (95% wool, 4.5% nylon, and 0.5% Lycra) [29], polymer/MWNT-coated Spandex yarn [30] and various textiles like cotton, and Lycra [31] are some examples. However, these sensors not only have exhibited limited stretchability ranging from 3 to 50%, but also their sensing ability to detect human motion has not be reported.

In this study, we developed a highly stretchable and sensitive strain sensor via spray layer-by-layer (spray-LbL) assembly of SWNTs on a commercialized nylon textile. By cutting commercial thigh-highs, nylon textiles were easily obtained at low price, and to the best of our knowledge, nylon of thigh-highs is firstly used for strain sensor. Nylon is elastic, tough, light-weight and resistant to abrasion [32], and it has good strain recovery compared to cotton [33]. To coat textile with SWNTs, which have extremely high electrical conductivity of 10^4-10^6 S cm^{-1} and a current carrying capacity of up to 10^9 A cm^2 [21,34,35], vacuum-assisted spray-LbL technique was used. It is a simple, low-cost, and rapid approach for creating uniform thin films [36,37]. The application of the vacuum could pull the water solution through the porous substrate by applied pressure drop, reinforcing adhesion of the materials on the substrate [36,38,39]. Therefore, the vacuum-assisted spray-LbL assembly could be coated on a surface and fill between textile fibers with SWNTs. The developed strain sensors exhibited excellent performance: high stretchability (100%) and high sensitivity, fast-response, durability over 1000 stretching/releasing cycles, and reliability. Further, the sensors were attached to the glove and sewn with the knee part of leg-

†To whom correspondence should be addressed.
E-mail: shjeong@knu.ac.kr
‡Both authors contributed equally to this work.

gings, successfully demonstrating the ability to recognize finger and knee movements.

EXPERIMENTAL

1. Plasma Treatment of Nylon Textiles

Knitted nylon textiles (90% nylon, 10% polyurethane) were obtained from commercial thigh-highs. Before treatment, the textiles (5×5 cm^2) were cleaned using acetone and ethanol for removing impurities, and then dried in oven at 100 °C for 10 min. Washed nylon textiles were modified with an oxygen plasma (Cute-B, Femto science, Korea) at a vacuum of 200 mTorr, and a 100 W discharge power with an exposure time of 10 min.

2. Functionalization of SWNT

To fabricate SWNT multilayer films, positively and negatively charged SWNT should be prepared by following the published protocols [40,41]. First, negatively charged SWNTs were made by oxidation with a mixture of concentrated acid (3/1 v/v, 80% H_2SO_4, 60% HNO_3) to create carboxylic groups (-COOH). Specially, 0.5 g SWNTs (91% purity, length 1-3 μm, outer diameter 2 nm, Soochow Hengqiu Graphene Technology Co., Ltd., China) were placed in a round bottom flask containing 40 ml of the acidic mixture and heated at 70 °C for 2 h under reflux. Next, the oxidized SWNTs were washed several times with deionized water (D.I water, 17.8 MΩ cm) by filtration using polycarbonate membrane with a pore size of 0.05 μm (Whatman, UK), and then dried in oven at 100 °C overnight. To modify the SWNTs with positively charged ammonium ions (SWNT-NH_3^+), carboxylated SWNT solution (100 ml, 0.5 mg ml^{-1}) was used with excess ethylenediamine (10 ml) in the existence of 1 g of 1-[3-(Dimethylamino)propyl]-3-ethylcarbodiimide methiodide (EDC). The resulting solution was dialyzed for a few days to remove any residuals and byproducts.

3. Fabrication of Conductive SWNT/Nylon Textiles via Vacuum-assisted Spray-LbL Assembly

For conformal coating of SWNT films on nylon textiles, vacuum-assisted spray-LbL assembly was used. The plasma-treated nylon textile was fixed on a holder of vacuum filtration apparatus that had been connected to an adjustable house vacuum via rubber tubing. Then, a funnel was put on the holder to prevent SWNT ink from spattering outside. The charged SWNT powders were dispersed in D.I water and ultrasonicated for several hours prior to spray-LbL assembly. The charged SWNT solutions were sprayed using an automated sprayer system driven by N_2 gas (20 psi). SWNT-NH_3^+ solution was first sprayed for 3 s at rate of 0.3 ml s^{-1} and drained for 10 s under vacuum. Continuously, D.I water was also sprayed for the same condition. This half cycle was repeated for SWNT-COO^- solution, and total cycle was repeated for the number of bilayers (n) studied. Finally, the obtained conductive SWNT/nylon textile was dried at 100 °C for 10 min to remove the moisture.

4. Fabrication of SWNT/Nylon Textile Strain Sensors

To fabricate the strain sensors, the SWNT/nylon textiles were cut into 1.5×1 cm^2. 3×1 cm^2 of two copper tapes were connected to the both ends of SWNT/nylon textiles with 1 cm in separation. Silver paste (Silbest p-248) was smeared at the contacting site between the conductive textile and copper tapes to reduce contact resistance.

5. Characterization

The morphology of SWNT/nylon textile was investigated by field emission scanning electron microscope (FE-SEM, S-4500, Hitachi Hi-Tec., Japan). The functional group of SWNTs was analyzed using Fourier transform-infrared spectroscopy (FT-IR, Frontier, Perkin Elmer, USA). The sheet electrical resistance of SWNT/nylon textile was measured by four-point probes (Loresta-GP, MCP-T610, Japan). The electromechanical behavior of SWNT/nylon textile sensors was observed by stretching devices consisting of custom built stretching stage and position controller software (PMC software). The out signal of strain sensors was measured by monitoring the resistance using a multimeter (Agilent 34401A, USA) during stretching test.

RESULTS AND DISCUSSION

The fabrication process of SWNT/nylon textile by spray-LbL assembly is schematically illustrated in Fig. 1(a). Nylon surfaces are not only difficult to wet but have poor adhesion with other substances because of their low surface energy and poor chemical reactivity and a weak cohesion layer at the surface [32,42]. Therefore, nylon textile was first treated with oxygen plasma to enhance the interactions between SWNTs and nylon surfaces by increasing surface activation energy of nylon [43]. In comparison with the pristine textile, the plasma-treated textile has many pits on the surface (see Fig. S1(a), (b) in the Supplementary data). It results in the increase of surface roughness and facilitates the attachment of CNTs onto the surface [42]. To confirm the surface functional groups on the modified textile, FT-IR analysis was performed (see Fig. S1(c) in the Supplementary data). After oxygen plasma treatment, absorption bands at 1,236 and 1,740 cm^{-1}, which can be assigned to C-O and C=O stretch, respectively, appeared intensively. These intense peaks indicate the successful incorporation of oxygen functionalities on the textile surface.

Then, to create electrostatic assembly of SWNT films on the plasma-treated textile, negatively and positively charged SWNT solutions were prepared through chemical functionalization of SWNTs (see Fig. S2(a) in the Supplementary data). Carboxyl groups were created at the ends of unmodified SWNTs through acid oxidation to prepare negatively charged SWNTs (SWNT-COO^-). Positively charged SWNTs containing of free amine groups (SWNT-NH_3^+) were prepared by introducing amine groups through a carbodiimide-mediated coupling reaction between SWNT-COO^- and ethylenediamine. FT-IR analysis was performed to verify the functionalization of SWNTs (see Fig. S2(b) in the Supplementary data). In the spectrum of SWNT-COO^-, the peaks at 1,693 and 1,126 cm^{-1} are referred to the C=O and C-O stretch of carboxylic (-COOH) groups. The spectrum of SWNT-NH_3^+ shows two peaks at 1,621 and 1,560 cm^{-1} that are attributed to the C=O and N-H stretch of secondary amide functional groups, suggesting the successful formation of amide bonds. The appearance of an absorption band at 1,452 cm^{-1} indicates the presence of -CH_2 group in ethylenediamine. With these functionalized SWNTs, conformal (SWNT-NH_3^+/SWNT-COO^-)$_n$ films were coated by sequentially spraying SWNT-NH_3^+ and SWNT-COO^- solutions onto the plasma-treated nylon textiles.

Fig. 1(b)-(f) show a series of SEM images consisting of the tex-

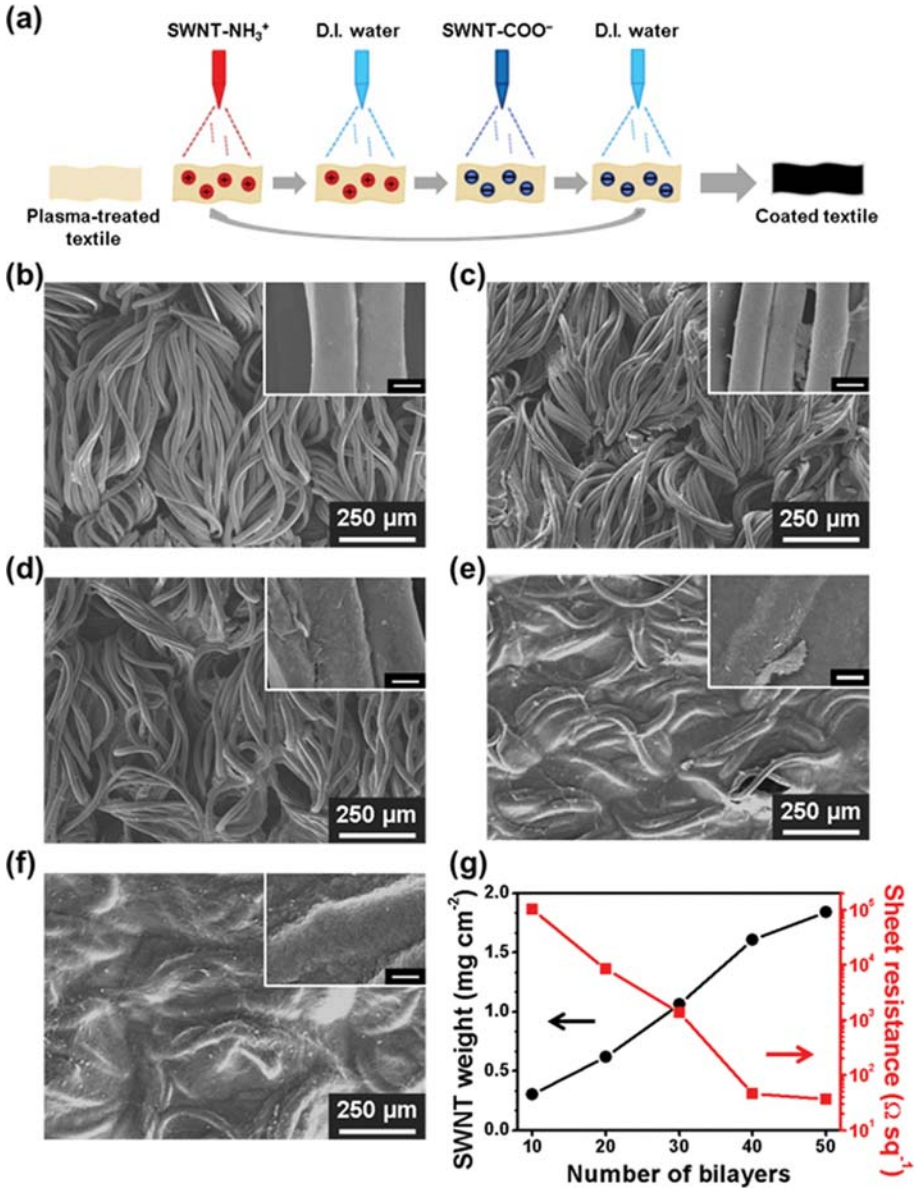

Fig. 1. (a) Schematic illustration for preparation processes of an SWNT/nylon textile using spray-LbL assembly. (b)-(d) SEM images of SWNT/nylon textiles fabricated with different bilayers numbers of: (b) 10, (c) 20, (d) 30, (e) 40, and (f) 50. Each inset shows high magnification of SEM image. Scale bar: 10 μm. (g) The effect of number of bilayers on SWNT weight [mg cm^{-2}] (black) and sheet resistance (red) of SWNT/nylon textiles.

tiles coated with 10, 20 30, 40, and 50 bilayers of (SWNT-NH_3^+/SWNT-COO^-) film, respectively. The SEM images clearly show that the SWNT loading increases with the number of deposited layers, gradually covering the nylon fibers and filling the gaps between the fibers. At n=40, the gaps are almost blocked with SWNTs, and the surface becomes relatively smoother at this point. At n=50, the morphology of underlying fibers is not visible, indicating formation of thick SWNT film. It is noticed that the electrostatic interaction between positively and negatively charged SWNTs, which have high degree of ionization, is the major driving force for the growth of the SWNT assembly on the textile. Fig. 1(g) displays the cumulative weight of (SWNT-NH_3^+/SWNT-COO^-) films on the textile and the sheet resistance of the SWNT/nylon textiles as a function of the number of bilayers. The SWNT weight increased almost linearly as the number of bilayers on the surface increased, indicating that each LbL process adds an approximately equivalent amount. However, the sheet resistance decreased dramatically by ~91.7% between 10 and 20 bilayers, while a gradual decline of only ~8.2% could be observed with further increasing number of LbL cycles. The initial significant drop in resistance represents that added SWNTs efficiently constructed electrically conductive networks, and the declining tendency of resistance suggests that more conductive paths are assembled as the amount of accumulated SWNTs increases. However, as more bilayers are added, the resistance variation becomes more sluggish because inevitable junction resistance increases with increasing SWNT-SWNT connection [21]. By 50 bilayers,

the SWNT/nylon textile attained the sheet resistance of ~36.7 ohm sq^{-1}, which is lower than that of 40-bilayer of SWNT/nylon textile (~46.1 ohm sq^{-1}). This is because the 50 bilayers of SWNT films on textiles are analogous to a bulk material [21]. During the process of layer-by-layer deposition of oppositely charged SWNTs on the surface of Nylon textile, excess SWNTs, which were not covalently bonded, were thoroughly removed by vigorous washing. Therefore, it is expected that individual SWNTs seldom are detached from the textile resulting in no penetration of detached SWNTs into the human skins. Also, several studies have shown that CNTs is not related to skin irradiation and allergic risks. However, some studies showed that dermal exposure to SWNTs leads to dermal toxicity to skin due to accelerated oxidative stress which is triggered by the metal catalyst in SWCNTs [44]. Because of the non-toxicity, and biocompatibility of PDMS to human skin [45], a biocompatible coating of our strain sensors with PDMS could limit potential harmful effect.

Next, we investigated the influence of the number of bilayers on the strain sensing performance of the SWNT/nylon textile sensor. Fig. 2(a) shows the relative resistance change ($\Delta R/R_0$) of five SWNT/nylon textile sensors, indicating different n according to applied strain ranging from 0 to 100%. The increment in resistance of all the sensors appeared with increasing applied strain due to the separation of SWNT-SWNT junctions. Although the sensors with SWNT films of 20 and 30 bilayers could operate up to 100% tensile strain, 10, 40 and 50 bilayers of SWNT/nylon textiles could not survive up to 50, 65 and 50% strain, respectively. In the case of n=10, the resistance rapidly increased at 25% strain, which is attributed to the lack of conducting path as a result of a little amount of SWNT on the surface. On the other hand, when n=50, the textile could not support SWNT film under stretching because the SWNT film covering the surface was overly thick. Therefore, the 50-bilayer film has difficulty in accommodating the tensile strains, resulting in fracture of the SWNT films at large strains (see Fig. S3 in the Supplementary data). The fractures of the SWNT films are directly related to the loss of electrical conductivity of the strain sensors. To monitor large-scale human body motions, the strain sensors should be capable of detecting a wide range of strains. Therefore, 10, 40 and 50 bilayers of films are not suitable for wearable strain sensors because of their limited stretchability.

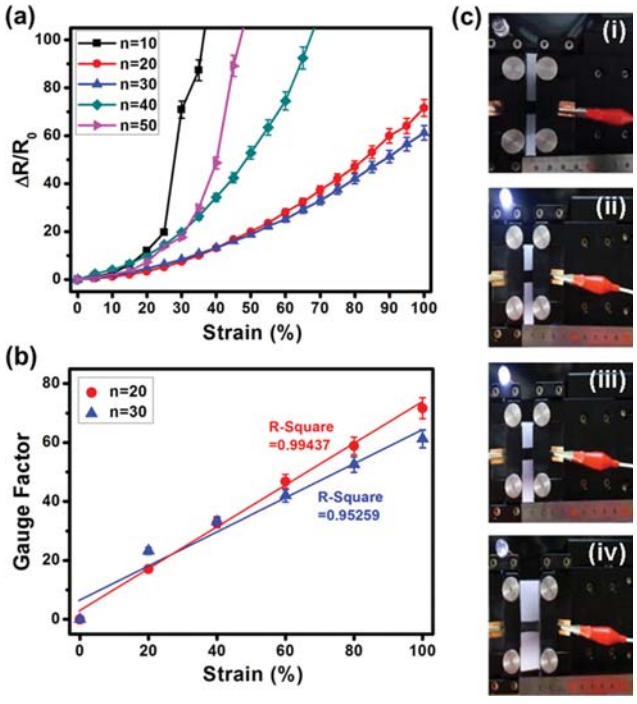

Fig. 2. (a) Relative resistance change ($\Delta R/R_0$) of SWNT/nylon textile fabricated with different numbers of bilayers (n). (b) Gauge factor of the strain sensors with different numbers of bilayers of 20 and 30 according to tensile strain. (c) Optical images of LED integrated circuit with the strain sensor (SWNT/nylon-20): (i) disconnected with the sensor, under (ii) 0, (iii) 50, and (iv) 100% strain.

To compare the sensitivity of 20 and 30 bilayer of SWNT/nylon textiles, which could stretch to 100%, the gauge factors of them were calculated from the data in Fig. 2(a) and these values are plotted in Fig. 2(b) as a function of tensile strain. The 20 bilayers of SWNT/nylon textile exhibited a gauge factor as high as 72 at 100% strain, which is higher than those of sensors with 30 bilayers (61.2). It indicates that lower SWNT loading makes the sensors more sensitive due to fewer electrical connections. This behavior is in good agreement with other studies [23,46,47]. For example, Hempel et al. [46] compared the strain sensitivities of graphene film-based strain sensors composed of different graphene flake density and lower flake density induced higher sensitivity.

Furthermore, the gauge factor of 20-bilayer SWNT/nylon textile is superior to other CNT-based strain sensors recently reported in the literature: CNT yarns on 100% prestrained Ecoflex (gauge factor of 64, stretchability of >900%) [22]; sandwich-liked stacked film of PU-poly(3,4-ethylenedioxythiophene) polystyrenesulfonate (PEDOT : PSS)/SWNT/PU-PEDOT : PSS (gauge factor of 62, stretchability of 100%) [23]; SWNT films on PDMS using LbL assembly (gauge factor of 15, stretchability of 80%) [21]; aligned MWNT/elastomer composites (gauge factor of >10, stretchability of 200%) [20]. All these sensors could not achieve both high stretchability (>100%) and high sensitivity (gauge factor of 72).

In addition, to visually confirm the ability of the sensor to sustain electrical conductivity even under high strain, 20 bilayers of SWNT/nylon textile were connected in series in a battery-powered (3 V) light-emitting diode (LED) circuit (Fig. 2(c)). Although the brightness of the LED was reduced due to increased resistivity under the stretched state, the LED remained lit when the sensor was stretched to 100%, indicating maintained conducting path. For both high stretchability and high sensitivity (gauge factor), we chose to focus on 20-bilayer films for further study of strain sensing performance.

We analyzed the responsivity of SWNT/nylon textile sensors by conducting dynamic stretch-and-release cyclic tests. First, the resistance change of SWNT/nylon textile was measured when it was stretched up to strain of 20% and released to its initial length. The sensor shows quite low hysteresis in Fig. 3(a). Also, the hysteresis decreased and was almost stabilized after the second cycle of stretch-and-release compared to the first cycle. Similar results were also reported elsewhere [48]. After stabilizing sensors by five stretching/releasing cycles at 20% strain level, cyclic stretching measure-

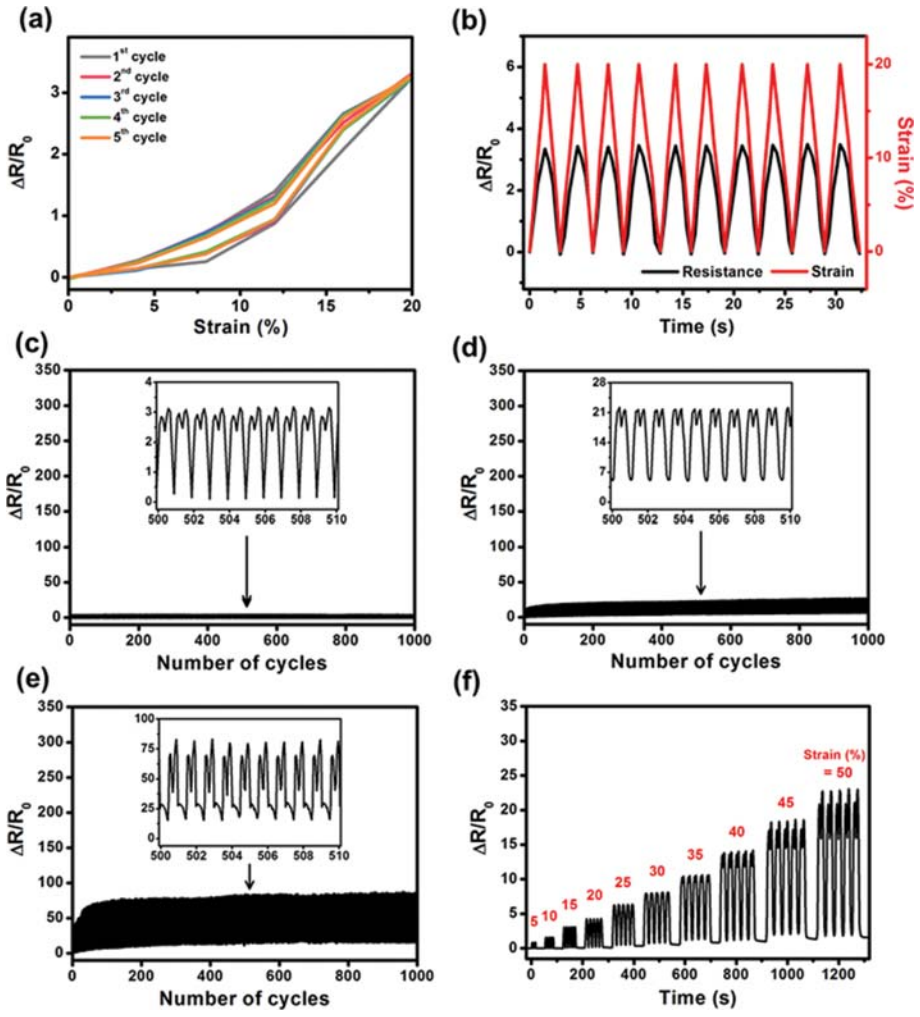

Fig. 3. (a) Hysteresis of 20-bilayer SWNT/nylon strain sensor while stretching 5 cycles within 20% strain range. (b) Time-dependent $\Delta R/R_0$ (black)of the sensors for 10 cycling between 0 and 20% strain (red). (c)-(e) $\Delta R/R_0$ of the sensors for 1000 cycles with different maximum strains of (c) 20, (d) 60 and (e) 100%. (f) Time-dependent ΔR/R0 of the sensors in response to strains ranging from 5 to 50% with repetitive stretching cycles (5 cycles per strain).

ment under strain ranging from 0 to 20% was applied. Fig. 3(c) shows excellent agreement between the resistance variation and the loading/unloading profile, indicating that the sensor could respond almost immediately to external deformation.

A strain sensor should endure large, complex, and dynamic strains for practical applications. To verify long-term durability and stability of the sensor, each resistance variation during repeated stretch-and-release process with a maximum strain of 20, 60 and 100% is shown in Fig. 3(c), (d) and (e), respectively. As shown in Fig. 3(c), the resistance increased only ~5% after 1,000 cycles from 0 to 20% strains. It seems that the peak and baseline of the $\Delta R/R_0$ were unchanged. Even under cyclic test at high strain of 60 and 100% (Fig. 3(d), (e)), the baseline was almost stable. On the other hand, the peak of the $\Delta R/R_0$ gradually increased with increasing number of cycles; it was eventually stabilized after ~100 cycles. Although the resistance increased ~35% at 100% strain experiment after 1,000 cycles, durability of the strain sensor was maintained. This good durability and recovery of conductivity might be attributed to the electrostatic interactions between the charged SWNTs. The strong electrostatic interactions can mechanically stabilize the SWNT film during stretching, preventing exfoliation of the film, and allow SWNTs to reconnect when the strain is released [21].

After stabilizing sensors by five stretching/releasing cycles at 50% strain level, the device was subjected to different levels of strain while its resistance was continuously measured. Fig. 3(f) shows $\Delta R/R_0$ of five cycles for strain of 5 to 50% with an incremental step of 5%. The response of the $\Delta R/R_0$ was proportional to the applied strains, reflecting the ability to detect the applied strain as low as 5%. In each cycle, the response was almost symmetrical and it could be fully recovered upon release. These results mean that the sensor has fast response time, excellent repeatability, and reliability. Compared with the linearity of relative resistance change ($\Delta R/R_0$) of SWNT/nylon textile sensors (n=20), which was measured without stabilizing process, in Fig. 2, stabilized sensors (Fig. 3(f)) by several stretching/releasing cycles showed improved linearity. However, the relation between strain and resistance still represents not a straight-line but somewhat similar to parabolic line. In most of the studies related to resistive-type CNT/polymer strain

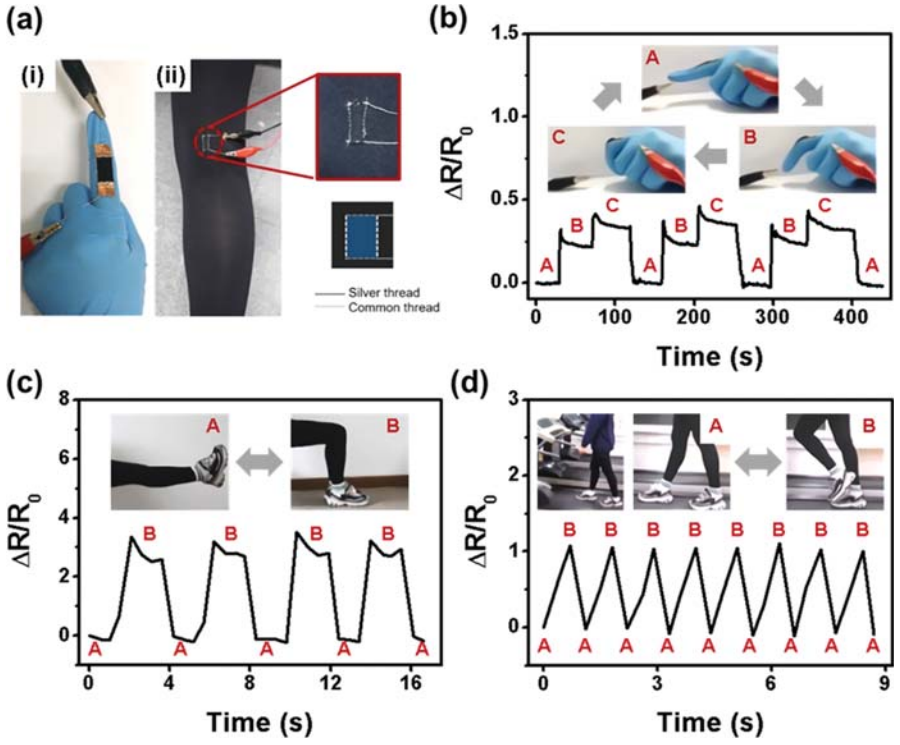

Fig. 4. (a) Photographs of 20-bilayer SWNT/nylon strain sensors (i) attached to index finger joint on the glove and (ii) sewed into knee joint part of the commercial leggings. (b)-(d) $\Delta R/R_0$ of the sensor for different human motions: (b) Finger bending motion, (c) knee bending motion, and (d) walking motion on a treadmill. Insets show the state points of finger and knee during tests.

sensors, the relation between strain level and resistance showed not perfect linearity but curved line similar to half side of quadratic function. Although the reason for this phenomenon is not elucidated, it might be attributed to the viscoelastic properties of polymeric materials and CNTs rearrangement.

Owing to its great advantages, such as high stretchability, sensitivity, fast response time, and long-term durability, the developed strain sensor can be used for wearable applications. As a demonstration, the strain sensor was attached onto a conventional latex glove to monitor the bending movements of the index finger (Fig. 4(a(i))). Fig. 4(b) shows the $\Delta R/R_0$ response of the sensor during the repeated bending/relaxation motion of the finger. When the finger was gradually folded, the resistance was accordingly increased and it recovered to the initial value once the finger was completely straightened. Similar degrees of finger bending under repeated cycles resulted in similar values of $\Delta R/R_0$, enabling accurate detection of bending motion.

In addition, 20-bilyaer SWNT/nylon textile can be easily integrated to clothes for a wearable system. Unlike other CNT-based strain sensors that were attached on the surface of clothes for motion detection [1,49], the SWNT/nylon textile was sewn with the knee part of the leggings, as shown in Fig. 4(a(ii)). When sewing the SWNT/nylon textile, non-conductive and silver-coated yarns were used. The responses of the $\Delta R/R_0$ were measured during motions including bending and walking on the treadmill at constant speed (3 km/h) (Fig. 4(c), (d)). The sensor exhibited high repeatability to strain variation induced by extension and flexion of the knee. The different motions generated different peak values of the $\Delta R/R_0$ and distinct signal patterns; therefore, they could be distinguished, with just one sensor. The successful realization of wearable strain sensors for monitoring body motions demonstrates the feasibility for practical application in sportswear, healthcare, and human-friendly rehabilitation.

CONCLUSIONS

We developed a highly stretchable and sensitive strain sensor based on SWNT-coated nylon textile. SWNT film was uniformly coated on the textile via vacuum-assisted spray-LbL assembly that is simple and fast. The SWNT weight and sheet resistance of SWNT/nylon textile were controlled by number of LbL cycles. Due to the flexibility of textile and electrostatic interactions between charged SWNTs, 20-bilayer SWNT/nylon textile exhibited high stretchability of 100%, high sensitivity (gauge factor of ~72), and durability over 1000 stretch-and-release cycles. We confirmed that this sensor could detect bending motions of a finger. In addition, the SWNT/nylon textile was simply sewed with the leggings and demonstrated the capability of detecting knee movements. This result suggests that our wearable strain sensor can be simply integrated to various clothes. We believe that this study could provide a meaningful approach to realizing wearable strain sensors for monitoring human motions.

ACKNOWLEDGEMENT

This research was supported by the Sports Promotion Fund of Seoul Olympic Sports Promotion Foundation from Ministry of

Culture, Sports and Tourism.

SUPPORTING INFORMATION

Additional information as noted in the text. This information is available via the Internet at http://www.springer.com/chemistry/journal/11814.

REFERENCES

1. T. Yamada, Y. Hayamizu, Y. Yamamoto, Y. Yomogida, A. Izadi-Najafabadi, D. N. Futaba and K. Hata, *Nat. Nanotechnol.*, **6**(5), 296 (2011).
2. I. Kang, M. J. Schulz, J. H. Kim, V. Shanov and D. Shi, *Smart Mater. Struct.*, **15**(3), 737 (2006).
3. V. Eswaraiah, K. Balasubramaniam and S. Ramaprabhu, *J. Mater. Chem.*, **21**(34), 12626 (2011).
4. T. Giorgino, P. Tormene, F. Lorussi, D. De Rossi and S. Quaglini, *IEEE Trans. Neural. Syst. Rehabil. Eng.*, **17**(4), 409 (2009).
5. P. Calvert, D. Duggal, P. Patra, A. Agrawal and A. Sawhney, *Mol. Cryst. Liq. Cryst.*, **484**(1), 291 (2008).
6. C. Cochrane, V. Koncar, M. Lewandowski and C. Dufour, *Sensors*, **7**(4), 473 (2007).
7. K. K. Kim, S. Hong, H. M. Cho, J. Lee, Y. D. Suh, J. Ham and S. H. Ko, *Nano Lett.*, **15**(8), 5240 (2015).
8. M. Amjadi, A. Pichitpajongkit, S. Lee, S. Ryu and I. Park, *ACS Nano.*, **8**(5), 5154 (2014).
9. C. Yan, J. Wang, W. Kang, M. Cui, X. Wang, C. Y. Foo, K. J. Chee and P. S. Lee, *Adv. Mater.*, **26**(13), 2022 (2014).
10. H. Tian, Y. Shu, Y.-L. Cui, W.-T. Mi, Y. Yang, D. Xie and T.-L. Ren, *Nanoscale*, **6**(2), 699 (2014).
11. Y. Wang, L. Wang, T. Yang, X. Li, X. Zang, M. Zhu, K. Wang, D. Wu and H. Zhu, *Adv. Funct. Mater.*, **24**(29), 4666 (2014).
12. T. Yamada, Y. Hayamizu, Y. Yamamoto, Y. Yomogida, A. Izadi-Najafabadi, D. N. Futaba and K. Hata, *Nat. Nanotechnol.*, **6**(5), 296 (2011).
13. D. J. Lipomi, M. Vosgueritchian, B. C. Tee, S. L. Hellstrom, J. A. Lee, C. H. Fox and Z. Bao, *Nat. Nanotechnol.*, **6**(12), 788 (2011).
14. S. Luo and T. Liu, *Adv. Mater.*, **25**(39), 5650 (2013).
15. W. Obitayo and T. Liu, *J. Sensors*, **2012**, 652438 (2012).
16. C. Stampfer, A. Jungen, R. Linderman, D. Obergfell, S. Roth and C. Hierold, *Nano Lett.*, **6**(7), 1449 (2006).
17. S. Tadakaluru, W. Thongsuwan and P. Singjai, *Sensors*, **14**(1), 868 (2014).
18. P. Slobodian, P. Riha, R. Benlikaya, P. Svoboda and D. Petras, *IEEE Sens. J.*, **13**(10), 4045 (2013).
19. M. Amjadi, Y. J. Yoon and I. Park, *Nanotechnol.*, **26**(37), 375501 (2015).
20. K. Suzuki, K. Yataka, Y. Okumiya, S. Sakakibara, K. Sako, H. Mimura and Y. Inoue, *ACS Sens.*, **1**(6), 817 (2016).
21. A. Vohra, P. Imin, M. Imit, R. S. Carmichael, J. S. Meena, A. Adronov and T. B. Carmichael, *RSC Adv.*, **6**(35), 29254 (2016).
22. S. Ryu, P. Lee, J. B. Chou, R. Xu, R. Zhao, A. J. Hart and S.-G. Kim, *ACS Nano*, **9**(6), 5929 (2015).
23. E. Roh, B.-U. Hwang, D. Kim, B.-Y. Kim and N.-E. Lee, *ACS Nano*, **9**(6), 6252 (2015).
24. M. Amjadi, A. Pichitpajongkit, S. Lee, S. Ryu and I. Park, *ACS Nano*, **8**(5), 5154 (2014).
25. M. Amjadi, K. U. Kyung, I. Park and M. Sitti, *Adv. Funct. Mater.*, **26**(11), 1678 (2016).
26. R. Ma, J. Lee, D. Choi, H. Moon and S. Baik, *Nano Lett.*, **14**(4), 1944 (2014).
27. S. Seyedin, J. M. Razal, P. C. Innis, A. Jeiranikhameneh, S. Beirne and G. G. Wallace, *ACS Appl. Mater. Interfaces*, **7**(38), 21150 (2015).
28. T. J. Kang, A. Choi, D.-H. Kim, K. Jin, D. K. Seo, D. H. Jeong, S.-H. Hong, Y. W. Park and Y. H. Kim, *Smart Mater. Struct.*, **20**(1), 015004 (2010).
29. M. in het Panhuis, J. Wu, S. A. Ashraf and G. G. Wallace, *Synth. Met.*, **157**(8), 358 (2007).
30. R. Zhang, H. Deng, R. Valenca, J. Jin, Q. Fu, E. Bilotti and T. Peijs, *Sens. Actuat. A- Phys.*, **179**, 83 (2012).
31. C. Robert, J. F. Feller and M. Castro, *ACS Appl. Mater. Interfaces*, **4**(7), 3508 (2012).
32. W. Zhang, L. Johnson, S. R. P. Silva and M. Lei, *Appl. Surf. Sci.*, **258**(20), 8209 (2012).
33. L. M. Castano and A. B. Flatau, *Smart Mater. Struct.*, **23**(5), 053001 (2014).
34. Z. Yao, C. L. Kane and C. Dekker, *Phys. Rev. Lett.*, **84**(13), 2941 (2000).
35. D. S. Hecht, L. Hu and G. Irvin, *Adv. Mater.*, **23**(13), 1482 (2011).
36. S. Y. Kim, J. Hong, R. Kavian, S. W. Lee, M. N. Hyder, Y. Shao-Horn and P. T. Hammond, *Energy Environ. Sci.*, **6**(3), 888 (2013).
37. K. Saetia, J. M. Schnorr, M. M. Mannarino, S. Y. Kim, G. C. Rutledge, T. M. Swager and P. T. Hammond, *Adv. Funct. Mater.*, **24**(4), 492 (2014).
38. P. A. Kralchevsky and K. Nagayama, *Langmuir*, **10**(1), 23 (1994).
39. K. C. Krogman, J. L. Lowery, N. S. Zacharia, G. C. Rutledge and P. T. Hammond, *Nat. Mater.*, **8**(6), 512 (2009).
40. S. W. Lee, B.-S. Kim, S. Chen, Y. Shao-Horn and P. T. Hammond, *J. Am. Chem. Soc.*, **131**(2), 671 (2008).
41. T.-K. Hong, D. W. Lee, H. J. Choi, H. S. Shin and B.-S. Kim, *ACS Nano*, **4**(7), 3861 (2010).
42. C. Canal, R. Molina, E. Bertran and P. Erra, *J. Adhes. Sci. Technol.*, **18**(9), 1077 (2004).
43. W. Zhang, L. Johnson, S. R. P. Silva and M. Lei, *Appl. Surf. Sci.*, **258**(20), 8209 (2012).
44. A. A. Shvedova, V. Castranova, E. R. Kisin, D. Schwegler-Berry, A. R. Murray, V. Z. Gandelsman, A. Maynard and P. Baron, *J. Toxicol. Environ. Health*, **66**(20), 1909 (2003).
45. A. Mata, A. J. Fleischman and S. Roy, *Biomed. Microdevices*, **7**(4), 281 (2005).
46. M. Hempel, D. Nezich, J. Kong and M. Hofmann, *Nano Lett.*, **12**(11), 5714 (2012).
47. J. J. Park, W. J. Hyun, S. C. Mun, Y. T. Park and O. O. Park, *ACS Appl. Mater. Interfaces*, **7**(11), 6317 (2015).
48. C. Park, H. Jung, H. Lee, S. Hong, H. Kim and S. J. Cho, *Sensors*, **18**(8), 2673 (2018).
49. G.-H. Lim, N.-E. Lee and B. Lim, *J. Mater. Chem. C*, **4**(24), 5642 (2016).

Supporting Information

Highly stretchable and sensitive strain sensors based on single-walled carbon nanotube-coated nylon textile

Yein Lee[*,‡], Juhyeon Kim[*,‡], Heeseon Hwang[**], and Soo-Hwan Jeong[*,†]

*Department of Chemical Engineering, Kyungpook National University (KNU), 80 Daehak-ro, Buk-gu, Daegu 41566, Korea
**Korea Institute of Robot and Convergence, 39 Jigok-ro, Nam-gu, Pohang-si, Gyeongsangbuk-do 37666, Korea
(*Received 22 October 2018 • accepted 21 February 2019*)

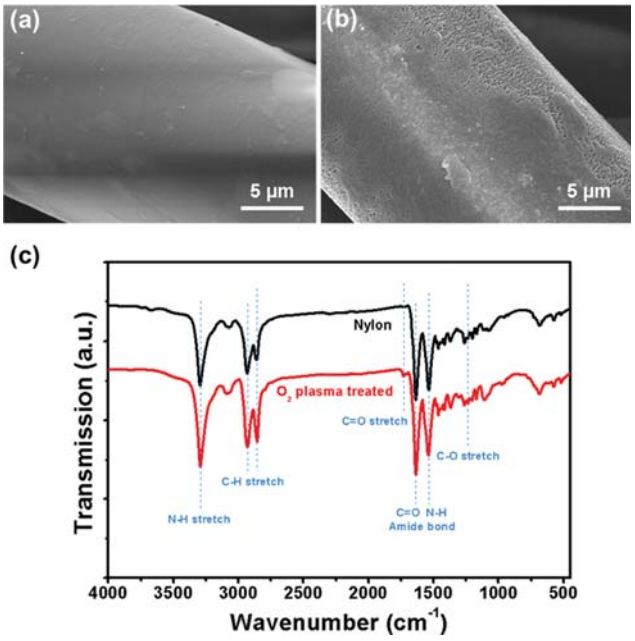

Fig. S1. (a)-(b) SEM images of nylon textiles: (a) Pristine and (b) plasma-treated. (c) FT-IR spectra of pristine and plasma-treated nylon textiles.

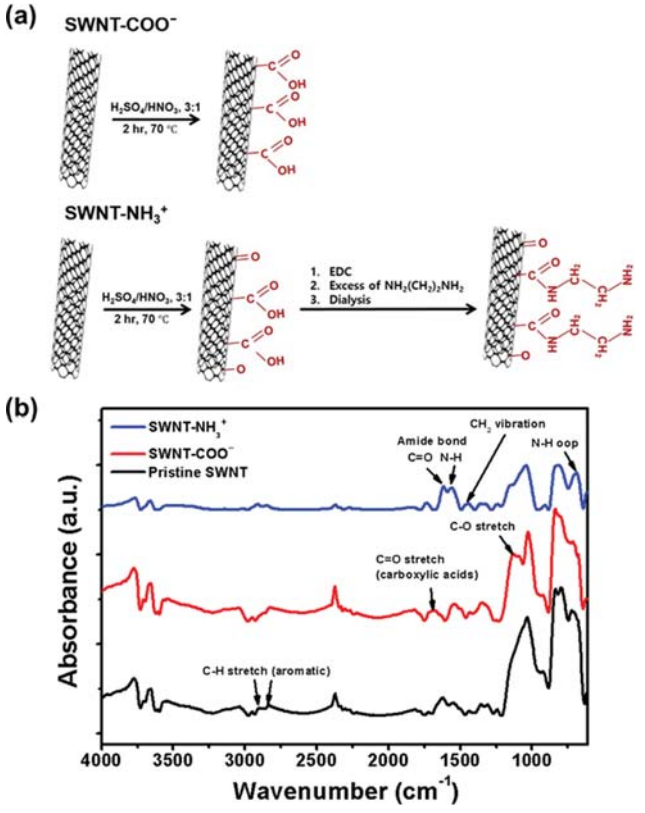

Fig. S2. (a) Schematic representation for functionalization of SWNTs: negatively charged SWNTs (SWNT-COO^-) and positively charged SWNTs (SWNT-NH_3^+). (b) FT-IR spectra of pristine SWNT, SWNT-COO^-, and SWNT-NH_3^+.

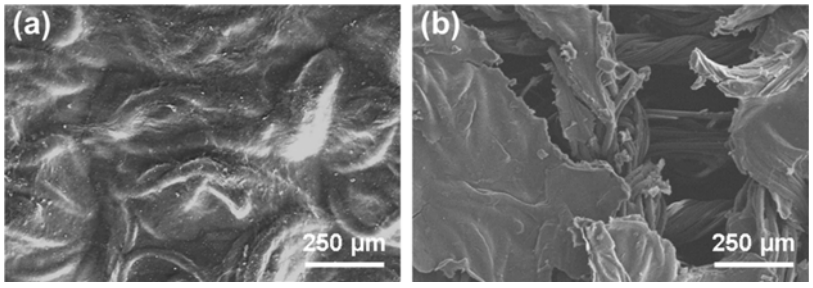

Fig. S3. SEM images of 50-bilayer SWNT/nylon textile (a) without strain and (b) at 70% strain.